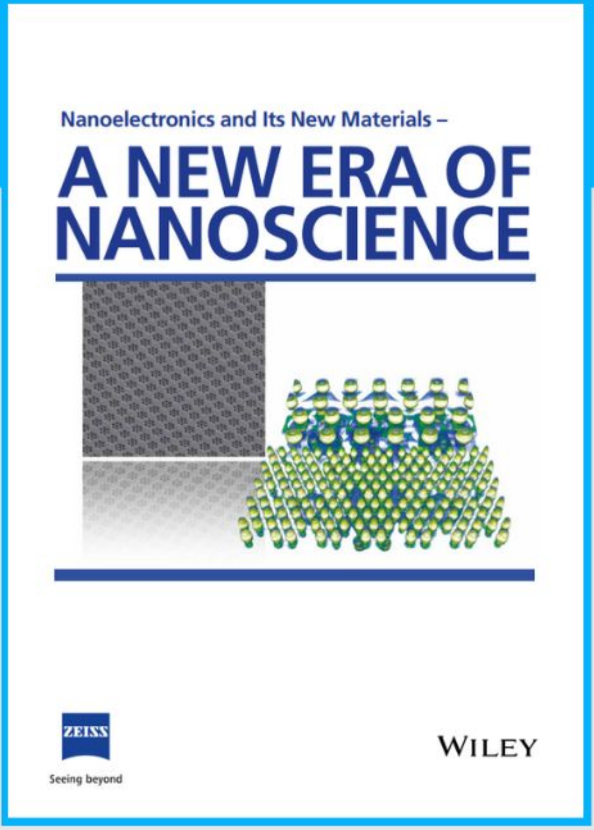
Nanoelectronics and Its New Materials –
A NEW ERA OF NANOSCIENCE
ZEISS
Seeing beyond
WILEY

Nitrogen-Doped and Sulfonated Carbon Dots as a Multifunctional Additive to Realize Highly Reversible Aqueous Zinc-Ion Batteries

*Tian-Bing Song, Zun-Hui Huang, Xi-Rong Zhang, Jia-Wen Ni, and Huan-Ming Xiong**

Aqueous zinc-ion batteries (ZIBs) using the Zn metal anode have been considered as one of the next-generation commercial batteries with high security, robust capacity, and low price. However, parasitic reactions, notorious dendrites and limited lifespan still hamper their practical applications. Herein, an eco-friendly nitrogen-doped and sulfonated carbon dots (NSCDs) is designed as a multifunctional additive for the cheap aqueous $ZnSO_4$ electrolyte, which can overcome the above difficulties effectively. The abundant polar groups (-COOH, -OH, $-NH_2$, and $-SO_3H$) on the CDs surfaces can regulate the solvation structure of Zn^{2+} through decreasing the coordinated active H_2O molecules, and thus redistribute Zn^{2+} deposition to avoid side reactions. Some of the negatively charged NSCDs are adsorbed on Zn anode surface to isolate the H_2O/SO_4^{2-} corrosion through the electrostatic shielding effect. The synergistic effect of the doped nitrogen species and the surface sulfonic groups can induce a uniform electrolyte flux and a homogeneous Zn plating with a (002) texture. As a result, the excellent cycle life (4000 h) and Coulombic efficiency (99.5%) of the optimized ZIBs are realized in typical $ZnSO_4$ electrolytes with only 0.1 mg mL^{-1} of NSCDs additive.

1. Introduction

Rechargeable aqueous zinc ion batteries (ZIBs) have attracted increasing attention widely owing to their distinctive advantages, such as outstanding safety, low toxicity, abundant raw materials, and relatively high energy density. Metallic Zn is employed as the anode for ZIBs because of its high theoretical specific capacity (820 mAh g^{-1} or 5855 mA h cm^{-3}) and low reduction potential (–0.76 V versus standard hydrogen electrode).[1–4] But Zn anodes in aqueous electrolytes always suffer from Zn dendrites, H_2 evolution reactions, and chemical corrosions (**Scheme 1**a), which heavily decrease the Coulombic efficiency (CE) of the anodes and the cycling lifetime of ZIBs. In detail, the growth of zinc dendrites without control will produce the "dead Zn", even puncture the separator, and short-circuit the battery ultimately. And the water-induced hydrogen evolution reaction (HER) might cause cell swelling and explosion. In addition, the local accumulation of OH^- often results in repulsive by-products like $Zn_4SO_4(OH)_6 \cdot xH_2O$. To overcome the above problems, some strategies have been developed recently, such as constructing artificial interfaces, employing Zn alloys, designing anode structures, and modifying electrolytes, etc.[5–9] Among them, introducing functional electrolyte additives seems to be the most convenient, economical, and efficient method. By far, various additives have been tested, including metal ions, organic molecules, and metal oxides.[10–13] But most of them could only play one role in inhibiting Zn dendrites growth, zinc corrosion, or side reaction, respectively. It is still a challenge to find a new additive to resolve the above problems once and for all.

Carbon dots (CDs) are well-known for their excellent photoluminescence and catalysis properties. Besides, they have also shown promising applications in both electrodes and electrolytes for energy storage devices.[14–17] Many CDs consist of graphited cores and abundant amorphous surfaces functional groups, indicating that there are plenty of adjustable active sites on CDs. Furthermore, CDs can be facilely synthesized in a large scale from simple precursors, and then dispersed homogeneously in electrolytes. These virtues endow CDs unique ability to combine with metal ions tightly, control the growth and morphology of inorganic compounds, and increase the conductivity of the composites.[18–20] Recently, graphene quantum dots (GQDs, one type of CDs) were prepared from graphite powder hydrothermally and added into the electrolyte for ZIBs, which availably suppress the growth of zinc dendrites, and distinctly improve both the cycling performance and the reversibility of ZIBs.[21] In order to utilize the functional surfaces of CDs, CDs were synthesized with plenty of polar groups and decorated onto the Zn anode directly to optimize electrolyte/Zn interfaces, which could help more Zn^{2+} adsorbed onto the whole electrode, ameliorate the electric field distribution, endow the Zn anode with high hydrophilicity, eliminate the water-mediated side reactions and improve Zn^{2+} reaction kinetics in the meantime.[22,23] These few pioneers' work confirmed that CDs are able to play positive roles in ZIBs through the adsorption of Zn^{2+} and protection of Zn anodes.

T.-B. Song, Z.-H. Huang, X.-R. Zhang, J.-W. Ni, H.-M. Xiong
Department of Chemistry and Shanghai Key Laboratory of Molecular Catalysis and Innovative Materials
Fudan University
Shanghai 200438, P. R. China
E-mail: hmxiong@fudan.edu.cn

The ORCID identification number(s) for the author(s) of this article can be found under https://doi.org/10.1002/smll.202205558.

DOI: 10.1002/smll.202205558

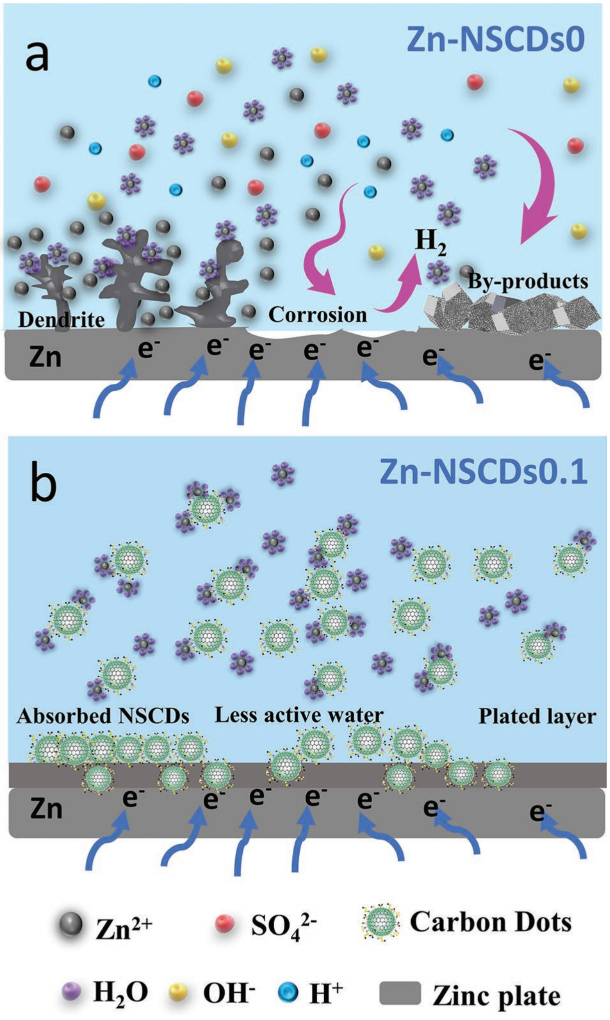

Scheme 1. Schematic diagrams for Zn deposition in 2 M $ZnSO_4$ electrolyte with and without NSCDs additive, respectively. a) Severe corrosion, hydrogen evolution and dendritic growth occur in the 2 M $ZnSO_4$ electrolyte during electrochemical cycling. b) The above disadvantages are suppressed by adding only a small amount of NSCDs in the $ZnSO_4$ electrolyte.

Since both the functional surface and the internal composition of CDs make positive senses toward ZIBs, it is necessary to construct the core and the shell of CDs synergistically for the optimal performance. Besides, adding CDs into the electrolyte is much more facile than coating them onto the Zn anode, indicating that the adsorption ability of CDs towards Zn should be improved from two aspects (core and shell). On the basis of the above inference, we design a new kind of CDs (NSCDs) as an additive for the typical $ZnSO_4$ aqueous electrolyte of ZIBs, which are doped with nitrogen inside and sulfonated on the surface (Scheme 1b). The polar groups, the highly negative charges, and the nitrogen-doped structure of such NSCDs manifest synergistic effects in the electrolyte. The sulfonic groups and other polar groups (-COOH, -OH, and -NH_2) have strong adsorption ability to Zn^{2+}, which could regulate the solvation structure of Zn^{2+} to decrease the coordinated active water molecules, reduce the nucleate overpotential, suppress by-products like $Zn_4SO_4(OH)_6 \cdot xH_2O$ as well as H_2 evolution. Besides, the Zn anode prefers to absorb the negatively charged NSCDs than H_2O, and thus its contact with H_2O/SO_4^{2-} is blocked by the electrostatic shielding. Sulfonic groups on NSCDs coating can also reshape the Zn deposited layer and enhance the mobility of the Zn^{2+} by the coupled rotational motion. The N-doped structure and the sulfonic groups further induce a uniform electrolyte flux and realize smooth Zn deposition. As proved by various characterizations and computational analyses, our NSCDs are able to decrease the activity of water molecules, reduce parasitic reactions, restrain the growth of Zn dendrites and establish a suitable Zn-ion affinity in the meantime. After assembly with the NSCDs-incorporated $ZnSO_4$ electrolyte, the symmetric Zn//Zn cell shows the remarkable cyclic performance (4000 and 3000 h at current densities of 0.5 and 1 mA cm^{-2}, respectively), the superior interfacial stability and the dendrite-free morphology after the repeated plating/stripping. The corresponding Zn//Ti half-cell achieves a high average Coulombic efficiency of 99.5% after 1200 cycles, and the corresponding Zn//MnO_2 full cell displays excellent cycle stability after 600 cycles, much better than those control cells using the NSCDs-free $ZnSO_4$ electrolyte.

2. Results and Discussion

Experimentally, NSCDs were synthesized via a typical solvothermal method (**Figure 1**a), then the resulting solution was dropped into ethanol and centrifuged to collect the precipitate. Afterward, the precipitate was re-dissolved into water, dialyzed and freeze-dried to obtain NSCDs powder. The TEM and the inset HRTEM images of NSCDs (Figure 1b) reveal the nanoparticles are monodispersed with uniform sizes of ≈2 nm. The lattice spacing of NSCDs is ≈0.21 nm, agreeing well with the (100) planes of graphite. In addition, the XRD pattern of NSCDs (Figure S1a, Supporting Information) exhibits a broad peak ≈25°, corresponding to the typical (002) reflection of the graphite structure. In the FT-IR spectra (Figure 1c), the asymmetrical stretching vibrations of O=S=O at 1030 and 1205 cm^{-1}, as well as the stretching vibration of C–S at 615 cm^{-1}, are proofs of the sulfonic groups on NSCDs.[24,25] The absorption bands at 1780, 1713, 1650, and 1545 cm^{-1} are assigned to C=O (carboxyl and carbonyl), C=N, C=C and C—N bonds, respectively, indicating that NSCDs have nitrogen incorporated aromatic structures. As for the wide and strong absorption bands in the range of 3500–3300 cm^{-1} and 3600–3200 cm^{-1}, these FTIR signals are typical for the electronegative -OH, -COOH and -NH_2 groups, which verify that nitrogen atoms have been doped on NSCDs surfaces.[26–28] XPS measurements are conducted to study the element composition of NSCDs. The wide range of XPS survey confirms the presence of carbon, oxygen, nitrogen, and sulfur (Figure S1b, Supporting Information) in NSCDs. In the high-resolution spectra, N 1s (Figure 1d) can be deconvoluted into four peaks, assigning to amino N (21%), pyridinic N (24.3%), pyrrolic N (26.5%) and graphitic N (28.2%), respectively.[29] C 1s spectrum in Figure 1e can be included into more components, such as COOH, C=O, C–OH, C–S, C=N/C-N, and C=C/C–C species. For the S 2p spectrum in Figure 1f, two major components are ascribed to C–S at 166.4 eV and S=O at 168.1 eV,

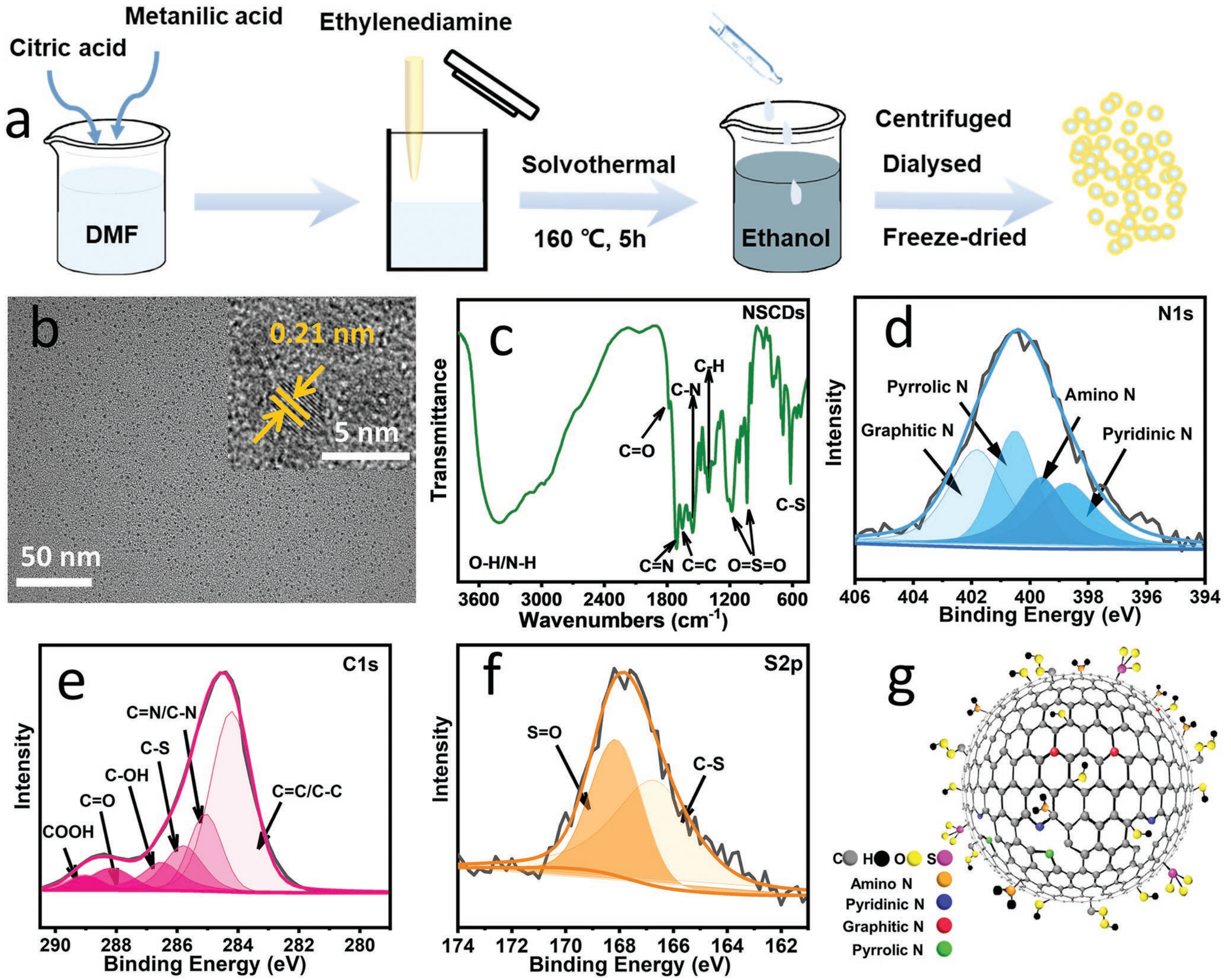

Figure 1. a) Schematic illustration of NSCDs synthesis. b) TEM image and the inset HRTEM image of NSCDs. c) FITR spectra of NSCDs. High resolution XPS analyses for d) N1s 2p, e) C1s and f) S2p of NSCDs, respectively. g) A schematic structure for NSCDs.

respectively.[30,31] Obviously, both FTIR and XPS analyses prove that our CDs have been doped with various N species and modified with -SO_3H groups. Moreover, NSCDs display a negative zeta potential value of –28 mV in water, suggesting that their surfaces are negatively charged (Figure S2, Supporting Information). The above characterization results confirm that electronegative NSCDs with doped N species and -SO_3H surface groups (Figure 1g) have been prepared successfully.

Different amounts of NSCDs were dissolved in 2 м $ZnSO_4$ electrolytes to obtain a series of samples named Zn-NSCDsx (x = 0–0.5). For example, when x = 0.1, the Zn-NSCDs0.1 sample has NSCDs concentration of 0.1 mg mL^{-1}. It should be noticed that the zeta potential value of Zn-NSCDs0.1 is close to 0 mV because of the adsorbed Zn^{2+} ions on NSCDs surfaces (Figure S2, Supporting Information). In Figure S3 (Supporting Information), Zn-NSCDs0 is colorless in daylight and has no fluorescence in UV light, while the other samples (x = 0.05–0.5) are yellow in daylight and show the typical blue fluorescence under UV light. The addition of NSCDs in the $ZnSO_4$ electrolyte will weaken the solvation interactions between Zn^{2+} and water, which can be verified by spectral analyses. First of all, the interactions between NSCDs and $ZnSO_4$ electrolytes were investigated by photoluminescence (PL) emission spectra. In **Figure 2**a and Figure S4 (Supporting Information), comparing the PL spectra of x mg mL^{-1} of NSCDs and the corresponding Zn-NSCDsx, the fluorescence intensities of all Zn-NSCDsx samples are significantly lower than the corresponding NSCDs samples. This phenomenon can be ascribed to the adsorption of Zn^{2+} on NSCDs, which leads to fluorescence quenching like many other metal ions. As a result, NSCDs also restrain electrostatic coupling between Zn^{2+} and SO_4^{2-} and influence the surrounding environment of Zn^{2+}.

In another way, the FTIR spectra were employed to further study the interactions between $ZnSO_4$ and NSCDs in the electrolytes. Figure 2b shows the typical absorption band of O–H stretching at 3093 cm^{-1} (Zn-NSCD0) shifts to 3206 cm^{-1} (Zn-NSCD0.5), which is close to that of the NSCDs solution. In Figure S5a (Supporting Information), the absorption band of O–H bending shifts from 1628 cm^{-1} (Zn-NSCD0.05) to 1643 cm^{-1} (Zn-NSCD0.5) gradually as the NSCDs concentration increases.[32,33] These blue shifts of O–H vibrations are owing to the perturbation of the hydrogen-bond network among the water molecules, i.e., the addition of NSCDs has weakened the interactions between Zn^{2+} and water molecules. Except for O–H vibrations, the S=O vibrations of SO_4^{2-} at 985 cm^{-1} in the $ZnSO_4$ electrolyte also blue shift when more and more NSCDs are added (Figure S5b, Supporting Information), indicating that the electrostatic coupling between Zn^{2+} and SO_4^{2-} are weakened by NSCDs. This time the free NSCDs sample exhibits no signal because the S=O vibrations of the -SO_3H groups in the NSCDs solution (0.5 mg mL^{-1}) are too weak to be detected.

Meanwhile, nuclear magnetic resonance (NMR) measurements on different solutions were conducted to investigate the effect of NSCDs in Zn-NSCD0 (Figure 2c). The ^{2}H peak of pure D_2O is 4.6465 ppm, which shifted obviously to 4.6757 ppm when NSCDs are dissolved to a concentration of 0.5 mg mL^{-1}. After dissolving $ZnSO_4$ to a concentration of 2 м, the ^{2}H peak of D_2O shifts to 4.7123 ppm, and the peak is broadened greatly. This phenomenon manifests that both the surrounding electron density and the shielding effect of D$^+$ in D_2O are decreased because the strong coordination between Zn^{2+} and D_2O reduces the free D_2O molecules in the solution. But when both NSCDs and $ZnSO_4$ are dissolved in D_2O to form a Zn-NSCDs0.5 solution, the ^{2}H peak moves back to 4.7012 ppm, suggesting that some confined D_2O molecules by Zn^{2+} are released again because NSCDs can adsorb Zn^{2+}.[5,34–36] Density functional theory (DFT) calculations were performed to compare the binding energies of Zn^{2+} to various binding sites of NSCDs (see Figure 2d; Figure S6, Supporting Information). The results show the nitrogen species have strong binding energies with Zn^{2+}, including graphitic N (–6.04 eV), pyrrolic N (–5.36 eV), pyridinic N (–5.30 eV), and amino N (–5.44 eV). And those surface groups on NSCDs also exhibit strong binding energies with Zn^{2+}, such as -OH (–5.04 eV), -C=O (–4.86 eV), -COOH (–5.32 eV), and -SO_3H (–6.42 eV). These values are all much larger than that of H_2O (–3.83 eV), which proves that the addition of NSCDs can regulate the Zn^{2+} solvation shells in water.

When a Zn foil is soaked in the Zn-NSCDs0.1, the NSCDs will be adsorbed on the Zn surface immediately. The as-prepared Zn foil is observed by a confocal laser scanning microscope (CLSM), which clearly shows the typical blue fluorescence of NSCDs (**Figure 3**a). Moreover, the FTIR spectrum

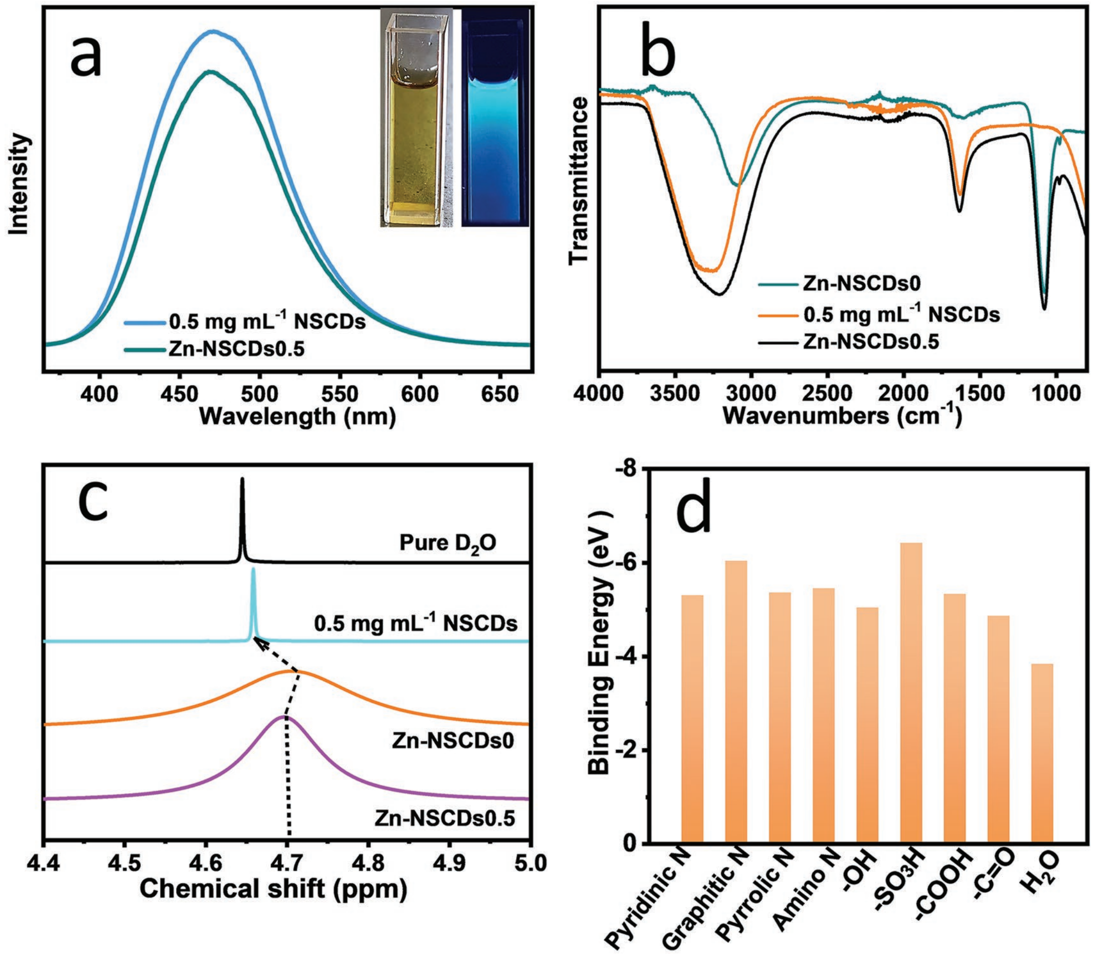

Figure 2. a) PL emission spectra of 0.5 mg mL^{-1} NSCDs and Zn-NSCDs0.5. The inset photos are the 0.5 mg mL^{-1} NSCDs solutions under daylight and UV light, respectively. b) FT-IR spectra of Zn-NSCDs0, 0.5 mg mL^{-1} NSCDs and Zn-NSCDs0.5 solutions. c) ^{2}H NMR spectra of D_2O, 0.5 mg mL^{-1} NSCDs, Zn-NSCDs0, and Zn-NSCDs0.5. d) Binding energies of Zn^{2+} absorbed on different function groups by DFT calculations.

of the as-prepared Zn foil (Figure 3b) shows similar bands with that of the NSCDs in the range from 800 to 1200 cm^{-1}, while the N–H/O–H band (≈3250 cm^{-1}) redshifts and the C=C band (≈1600 cm^{-1}) blueshifts. Such FTIR changes are attributed to the strong interactions between Zn and the polar groups of NSCDs.[37,38] In the contact angles measurements, tiny drops of the electrolytes are laid on Zn plates. In Figure S7 (Supporting Information), as the NSCDs concentration in the electrolytes increases from 0 to 0.5 mg mL^{-1}, the corresponding contact angle decreases gradually from 108° to 74°, which proves the wetting ability of the Zn electrode is significantly improved after adsorbed the NSCDs.[39] This result is consistent with the DFT calculations.

DFT calculations are also carried out to predict the Zn deposition process on the Zn electrode coated with NSCDs. Figure 3c displays the adsorption energies of H_2O and NSCDs on Zn (002) facet, respectively. The former is –18.73 kcal mol^{-1} while the latter is –51.26 kcal mol^{-1}, indicating that NSCDs are adsorbed upon Zn surface preferentially to isolate H_2O/SO_4^{2-} and restrain the side reactions. So after NSCDs coating, the nitrogen species and various functional groups on the Zn anode attract Zn^{2+} from the electrolyte (Figure 2d) and serve as zincophilic sites for Zn nucleation, which induces a uniform electrolyte flux and realizes a smooth Zn deposition. For example, -SO_3H groups are apt to release the proton and form -SO_3^- groups, which have strong electrostatic interaction with $[Zn(H_2O)_6]^{2+}$ to regulate the solvation structure of Zn^{2+}. Meanwhile, O atoms can rotate around the axis of the C–S bond to promote the Zn^{2+} migration with little energy in the tetrahedral structure of -C-SO_3^- in Figure 3d.[40,41] Therefore, the sulfonic groups on NSCDs can generate the electrostatic shielding effect to hinder side reactions, attract to Zn^{2+} from the electrolyte and help Zn^{2+} transfer to the Zn surface, which will induce a homogeneous Zn deposition on the anode finally.

Zn//Zn symmetric batteries were assembled with different Zn-NSCDsx (x = 0–0.5) to examine the effects of NSCDs in the electrolytes. Zn-NSCDs0.1 shows the optimal result in the ionic conductivity measurements (Table S1, Supporting Information), as well as in the electrochemical performance of the Zn//Zn symmetric batteries working at 0.5 mA cm^{-2} with a capacity of 0.25 mAh cm^{-2}. The cycle life was achieved to be 4000 h with small polarization using Zn-NSCDs0.1 (**Figure 4**a). Since the other Zn-NSCDsx showed the larger voltage polarization because of the instability of the Zn electrodes (Figure S8, Supporting Information), Zn-NSCDs0.1 was selected as the typical electrolyte for all of the controlled experiments. Afterward, the Zn//Zn symmetric cells were cycled with the Zn-NSCDs0 and Zn-NSCDs0.1 under various current densities and areal capacities respectively. The cells using Zn-NSCDs0.1 can stably cycle for over 3000 h at a current

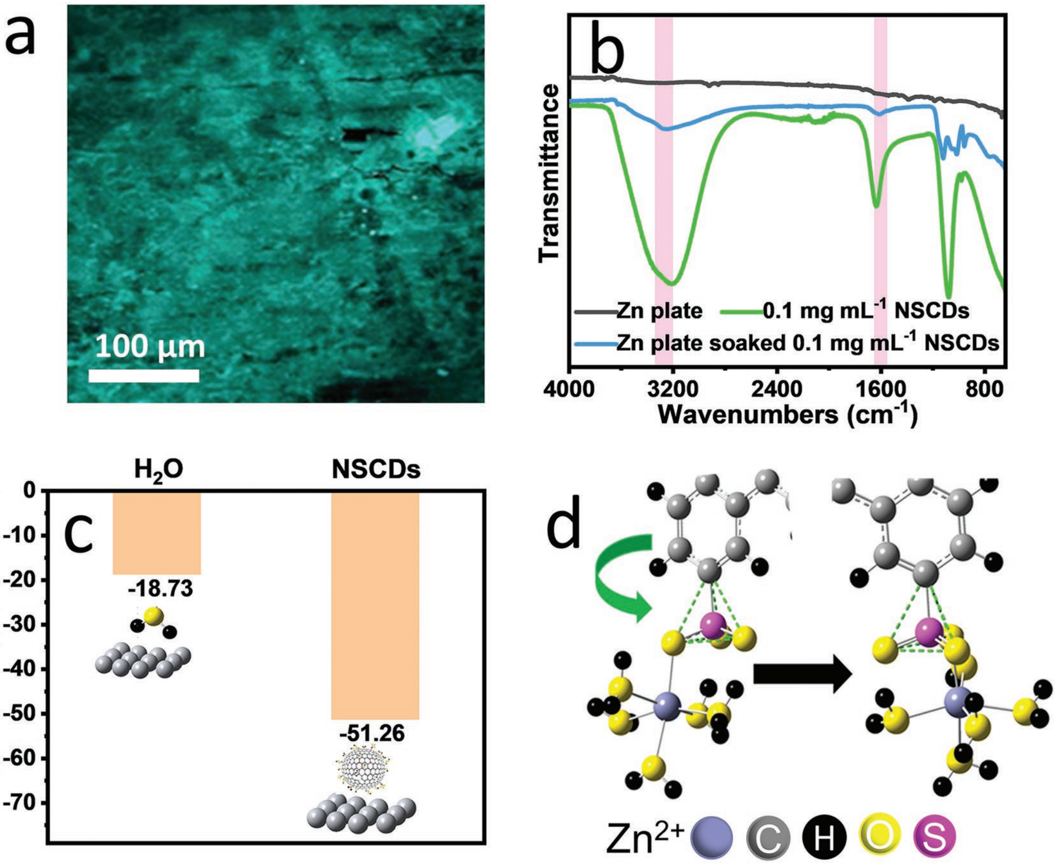

Figure 3. a) Confocal luminescence image of a Zn plate soaked in 0.1 mg mL^{-1} NSCDs. b) FT-IR spectra of Zn plate, 0.1 mg mL^{-1} NSCDs and Zn plate soaked in 0.1 mg mL^{-1} NSCDs. c) Absorption energy comparison of H_2O and NSCDs on the Zn (002) crystal plane. d) A schematic diagram of the paddle-wheel effect of the sulfonic group.

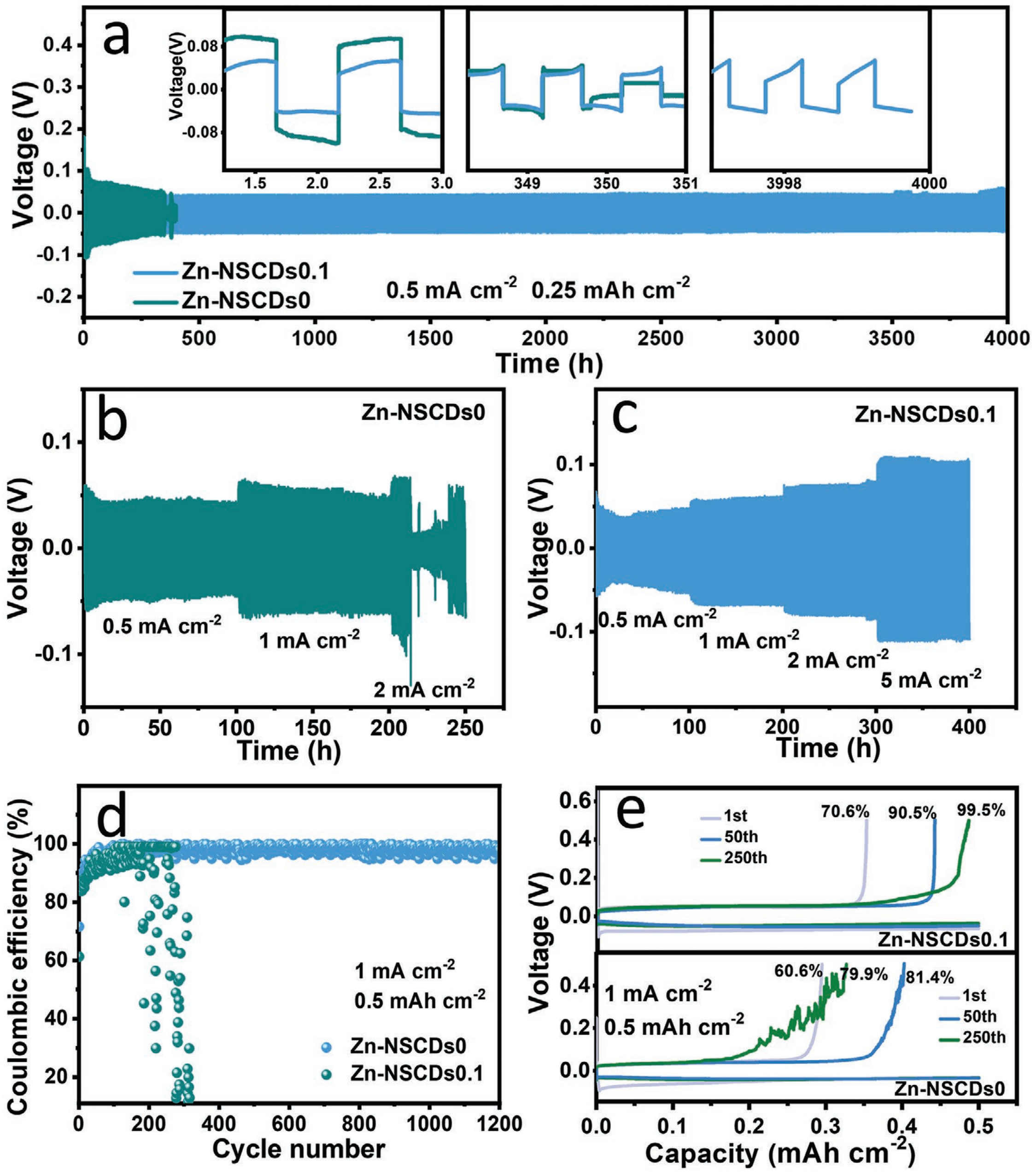

Figure 4. a) Comparison of long-term charging/discharging of Zn//Zn symmetric cell under current densities and areal capacities of 0.5 mA cm^{-2}, 0.25 mAh cm^{-2}. Rate performance of Zn//Zn symmetric cell in b) Zn-NSCDs0 and c) Zn-NSCDs0.1. d) Coulombic efficiency measurements of Zn//Ti cells using different electrolytes, and e) the corresponding voltage profiles at certain cycles.

density of 1 mA cm^{-2} with 0.5 mAh cm^{-2}, while the cells using Zn-NSCDs0 are short-circuited after 380 h of cycling under the same conditions (Figure S9, Supporting Information). Impressively, even at the current density of 5 mA cm^{-2} with a fixed capacity of 5 mAh cm^{-2}, the Zn//Zn symmetric cells are able to work over 1500 h, with stable charge/discharge behaviors and low-voltage hysteresis of only ≈220 mV (Figure S10, Supporting Information), which is superior to the cells using Zn-NSCDs0 (only 100 h and 350 mV) and most of the previous reports (Table S2, Supporting Information). Electrochemical impedance spectroscopy (EIS) measurements on the Zn//Zn cells were carried out after different cycles, using Zn-NSCDs0 and Zn-NSCDs0.1, respectively. Obviously, both the electrolyte resistances and the charge transfer resistances of the cell with Zn-NSCDs0.1 are much smaller than those of the cell with Zn-NSCDs0 (Figure S11 and Table S3, Supporting Information), which means the NSCDs-coating on Zn electrode has set up a good interface with the electrolyte owing to their abundant hydrophilic functional groups.

The rate performances of these batteries at various current densities are also compared during cycling. In Figure 4b, the cell using Zn-NSCDs0 presents the higher voltage hysteresis and the worse rate performance, even it is short-circuited at 2 mA cm^{-2}. But in Figure 4c, the cell using Zn-NSCDs0.1 delivers stable voltage profiles with a lower voltage polarization at 0.5, 1, 2, and 5 mA cm^{-2}, respectively. When the current density is increased from 0.5 to 5 mA cm^{-2}, this cell exhibits a steadily increasing voltage hysteresis of 94, 121, 155, and 210 mV, respectively. This phenomenon is owing to the NSCDs adsorbed on the Zn plate, which manipulates the Zn^{2+} distribution and reduces the nucleation barrier. Reversible plating/stripping tests in Zn//Ti coin-type cells were assembled to evaluate the Zn electrode performance. In Figure 4d,e, after the initial stage of the lattice fitting, the Coulombic efficiency of the cells working at 0.5 mA cm^{-2} with a capacity of 0.25 mAh cm^{-2} is close to 100% for the first 100 cycles. But after 125 cycles, the voltage of the Zn//Ti cells using Zn-NSCDs0 fluctuates violently and the corresponding CE is not stable. In contrast, the voltage of the Zn//Ti cells using Zn-NSCDs0.1 keeps stable for more than 1200 cycles, and its average CE is up to 97.6%, which means both the growth of Zn dendrites/by-products and many side-reactions are suppressed effectively by Zn-NSCDs0.1. Moreover, the CV measurements of Zn//Ti half-cells were also carried out to further investigate the effect of NSCDs on Zn stripping/plating behaviors. As shown in Figure S12 (Supporting Information), CV curves display similar pairs of reduction/oxidation in Zn-NSCDs0 and Zn-NSCDs0.1, indicating the negligible effects of NSCDs on the electrochemical reactions. It is worth noting that the Zn nucleation overpotential in Zn-NSCDs0.1 increased by 48 mV, suggesting the adequate driving force for the process of Zn nucleation and growth.

The morphology evolutions of Zn anodes were observed by SEM. The bare zinc plate looks like a smooth and flat surface (Figure S13a,b, Supporting Information), but zinc prefers to deposit on those slightly protuberant sites, where the nucleation and the corrosion take place in the subsequent cycling (Figure S13c,d, Supporting Information). **Figure 5** shows SEM and confocal luminescence images of Zn//Zn symmetric cells at 1 mA cm^{-2} and 0.5 mAh cm^{-2}. In Figure 5a, the Zn-NSCDs0 involved samples show the deposited Zn is porous and heterogeneous after 200 cycles. Many Zn nanoplates grow vertically and randomly on the Zn anode with various edges. Such inhomogeneous Zn deposition will grow gradually during cycles, and finally result in the large dendrites and more disorderly sheets which could pierce through the separator and cause short circuits (Figure 5b, after 400 cycles). In contrast, the Zn-NSCDs0.1 involved Zn deposition is dense and uniform after 200 cycles, which presents a smooth and flat morphology on the whole Zn electrode (Figure 5c). It should be emphasized that, even after 2000 cycles (Figure 5d), SEM images of Zn anodes with Zn-NSCDs0.1 still show flat and compact surface, while the corresponding EDX mapping results confirm the homogeneous coating of NSCDs. Since the only difference between Zn-NSCDs0 and Zn-NSCDs0.1 is the NSCDs component, the above dramatic changes are ascribed to the presence of NSCDs. The NSCDs have lots of sulfonic, carboxyl and carbonyl groups on the surfaces, so they can adhere to the Zn electrode and adsorb Zn^{2+} from electrolytes in the meantime. Such a homogeneous and tight NSCDs coating is able to hinder Zn dendrite growth and corrosion on one hand, and on the other, produce numerous Zn^{2+} nucleation sites to induce a homogeneous Zn deposition. Figure S14 (Supporting Information) clearly shows the different Zn deposition situations resulted from Zn-NSCDs0 and Zn-NSCDs0.1 by energy dispersive spectrometry (EDS) analyses respectively. For the sample derived from Zn-NSCDs0, obvious S element can be found in the Zn anode, indicating some by-products have been formed. In contrast, the Zn surface derived from Zn-NSCDS0.1 shows much weaker signal of sulfur, which is owing to the sulfonate on NSCDs, i.e., the side reactions involving SO_4^{2-} are suppressed by NSCDs on the Zn surface. The Zn deposition situation is further investigated by CLSM utilizing the fluorescent properties of NSCDs. Figure 5e–g shows confocal luminescence images of Zn deposition layer in Zn-NSCDs0.1 at 1 mA cm^{-2} and 0.5 mAh cm^{-2} after 5, 50, 100 cycles respectively, which present smooth and flat Zn plate layers. In contrast, the Zn electrodes with the Zn-NSCDs0 after 50 and 100 cycles at 1 mA cm^{-2} and 0.5 mAh cm^{-2} were immersed in NSCDs solution to adsorb NSCDs, and the as-treated Zn electrodes exhibit distinct dendrites and protuberance under CLSM (Figures S15 and S16, Supporting Information).

After 400 cycles at 0.5 mA cm^{-2} and 0.25 mAh cm^{-2}, the Zn electrodes were taken out for XRD measurements. In **Figure 6**a, the Zn plate from the Zn-NSCDs0 is similar with the commercial Zn plate, and their XRD patterns show the preferred growth along the (101) plane. Such a feature is ascribed to the Zn dendrites in literature. In contrast, the Zn plate from the Zn-NSCDs0.1 shows a different XRD feature that both the (002) and the (103) peaks increase relatively, thus the resulting Zn deposition becomes even and flat.[10] In addition, the XRD results also prove that the addition of NSCDs can effectively suppress side reactions since the peak intensity for the by-products was significantly reduced in Zn-NSCDs0.1 (inset of Figure 6a). The corrosion of the Zn plates in both electrolytes was evaluated by Tafel plots tests at a scan rate of 1 mV s^{-1}. In Figure 6b, the sample in Zn-NSCDs0.1 presents the smaller corrosion current (1.523 mA cm^{-2}) and the more negative corrosion potential (–0.98 V) than those in Zn-NSCDs0 (3.394 mA cm^{-2} and –0.97 V), indicating that NSCDs are able to enhance corrosion resistant ability of the Zn electrode.[42] In order to demonstrate the anti-corrosion effect of the NSCDs additive, we soaked the zinc foils in Zn-NSCDs0 and Zn-NSCDs0.1 for five days, respectively. As shown in the SEM images of Zn foils (Figure S17a,b, Supporting Information), abundant by-products attach to the Zn surface after soaking in Zn-NSCDs0, while no obvious corroded surface feature is observed in the sample soaked in Zn-NSCDs0.1. According to the XPS spectra (Figure S17c, Supporting Information), the content of sulfur element of Zn foils significantly increased in Zn-NSCDs0 in comparison with that in Zn-NSCDs0.1 due to the massive formation of by-products. Moreover, phase constitution of these by-products in Zn-NSCDs0 was identified as $Zn_4SO_4(OH)_6\cdot xH_2O$ by XRD measurements (Figure S17d, Supporting Information). The weaker XRD peak intensity of by-products from Zn-NSCDs0.1 further validates the alleviation of spontaneous corrosion when NSCDs are present.

It is well-known that both Zn corrosion and by-products formation are mainly attributed to the hydrogen evolution reaction (HER). When Zn plates are protected by NSCDs tightly, the HER is suppressed as well as the Zn corrosion. The linear

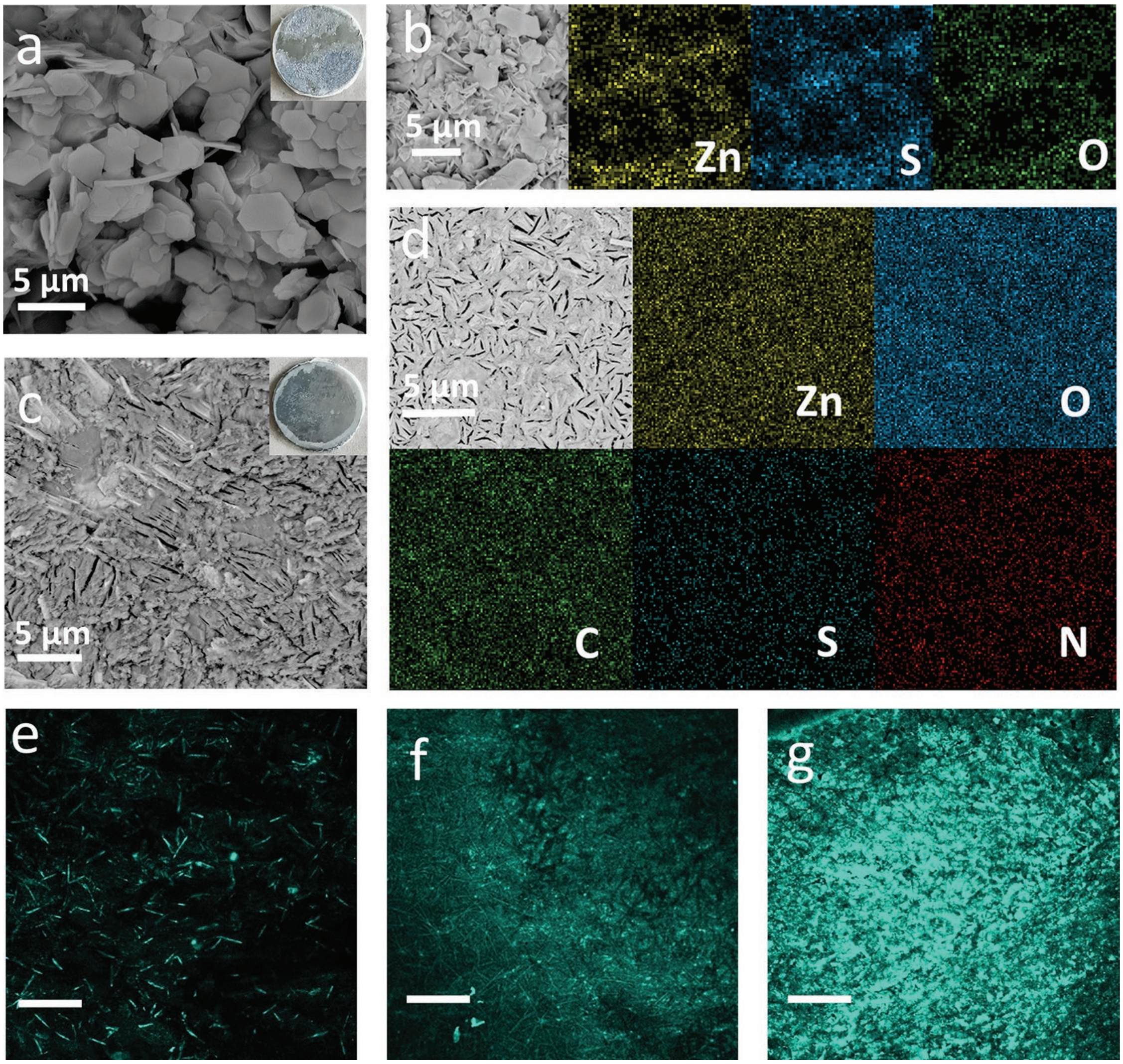

Figure 5. SEM and confocal luminescence images of Zn//Zn symmetric cells at 1 mA cm^{-2} and 0.5 mAh cm^{-2}. a) SEM images of Zn anodes after 200 cycles in Zn-NSCDs0. b) SEM image and EDX mapping of Zn anodes after 400 cycles in Zn-NSCDs0. c) SEM images of Zn anodes after 200 cycles in Zn-NSCDs0.1. d) SEM image and EDX mapping of Zn anodes after 2000 cycles in Zn-NSCDs0.1. Confocal luminescence images of Zn deposition layer in the Zn-NSCDs0.1 after e) 5 cycles, f) 50 cycles and g) 100 cycles, respectively. The white scale bars represent 100 µm.

sweep voltammetry (LSV) measurements in Figure 6c also confirms the suppressing impact of NSCDs on HER. In addition, the O_2 evolution at the higher overpotential is also suppressed by the NSCDs coating. In brief, the electrochemical stability of the Zn electrode is improved because of the tight protection of NSCDs with strong negative groups. Chronoamperometry (CA) was employed to analyze the Zn nucleation and growth, in which the variation of the current-time profile can reveal the surface change during Zn deposition. In Figure 6d, the current density in Zn-NSCDs0 presents a continuously increasing tendency within 300 s, corresponding to the 2D diffusion model in literature.[43,44] According to the minimum surface energy principle, those adsorbed Zn^{2+} tend to diffuse laterally along the surface, accumulate on the tips, and grow vertically into dendrites during the nucleation process. In contrast, a constant 3D diffusion process is observed in Zn-NSCDs0.1 after a short nucleation stage of ≈50 s, suggesting the dendrite growth stops immediately and the even deposition of Zn starts steadily. Moreover, CV curves of Zn//Zn symmetric cells are shown in Figure S18 (Supporting Information). The peak area of the redox reaction in Zn-NSCDs0.1 is larger than that in Zn-NSCDs0, indicating the electrochemical reactivity for Zn deposition is enhanced by adding NSCDs.

Zn//MnO_2 full cells were assembled and measured only using Zn-NSCDs0 and Zn-NSCDs0.1, in which β-MnO_2 was synthesized according to the literature[45] (see its XRD patterns and SEM image in Figure S19, Supporting Information). **Figure 7**a presents the cyclic voltammetry (CV) curves of the Zn//MnO_2 cells at a scan rate of 0.1 mV s^{-1} in the two electrolytes respectively, which share the similar behavior with distinct Mn-ion redox peaks. The addition of NSCDs did not change the redox reactions, implying that NSCDs were non-reactive in the full cells. Meanwhile, the influence of NSCDs additive on the inherent resistance of Zn//MnO_2 full cells was carried out by EIS tests in Figure S20a (Supporting Information). Zn//MnO_2 full cells with Zn-NSCDs0.1 has a

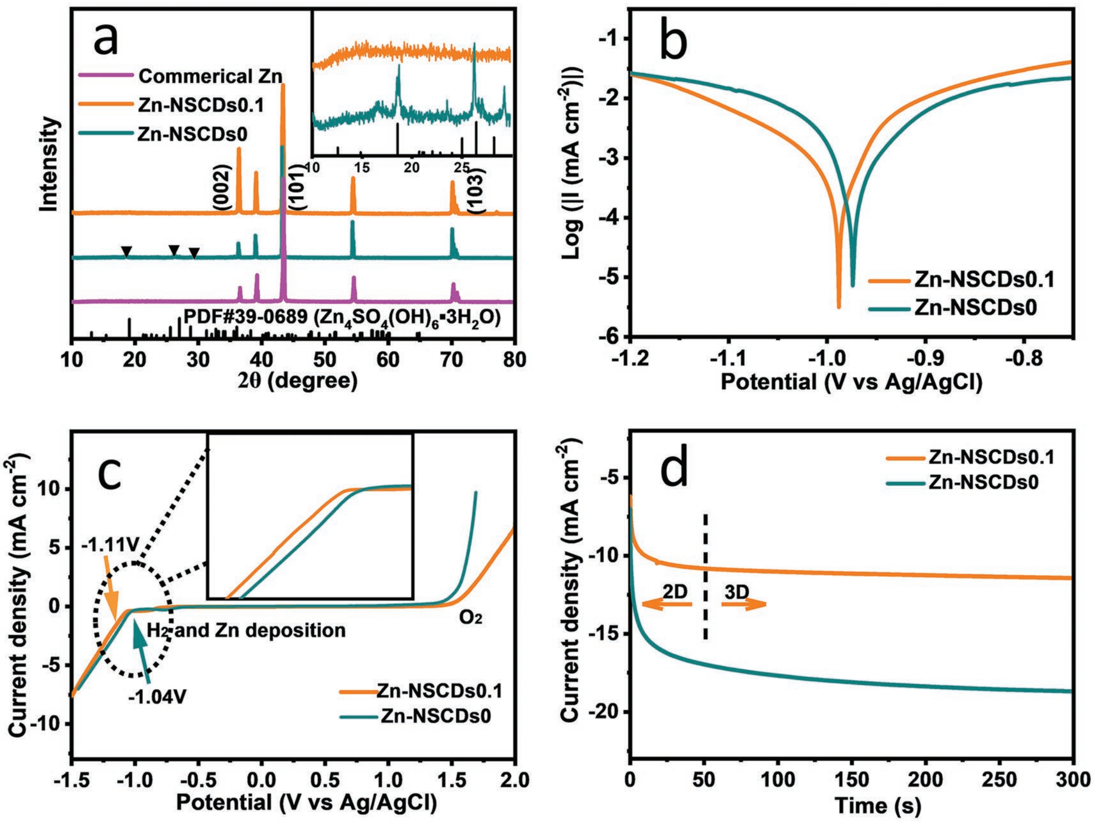

Figure 6. a) XRD patterns of zinc anodes after 400 cycles at 0.5 mA cm^{-2} and 0.25 mAh cm^{-2} in different electrolytes, respectively. b) Tafel plots representing corrosion behaviors in different electrolytes, respectively. c) LSV curves showing HER and OER (oxygen evolution reaction) at scan rate of 1 mV s^{-1}. d) Chronoamperometry curves indicating Zn^{2+} diffusion process of Zn electrode in different electrolytes, respectively.

smaller charge transfer resistance of 240.3 Ω than that of the Zn//MnO_2 full cell with Zn-NSCDs0 (411.6 Ω), revealing that NSCDs could effectively improve the ionic conductivity for fast redox reactions. And in Figure 7b,c, when different discharge C-rates of 0.1, 0.5, 1, 2, and 5 C are applied respectively, the rate performance of the cell using Zn-NSCDs0.1 is obviously better than that using Zn-NSCDs0. Furthermore, Figure 7d compares the cycling performance between two cells. The cell using Zn-NSCDs0 has a capacity of 74.4 mAh g^{-1} at 1 C. It is operated for only 350 cycles till the capacity retention decays to 49.8%. Afterward, a short circuit takes place due to the Zn dendrites. In contrast, the cell using Zn-NSCDs0.1 presents an initial reversible discharge capacity of 165 mAh g^{-1} at 1 C. After 60 cycles, its specific capacity decreases to 120 mAh g^{-1} with the corresponding capacity retention of 72.7%, while these values keep stable after more than 600 cycles at room temperature. In addition, we used a higher rate of 10 C to test the cycling performance of Zn//MnO_2 cells in both electrolytes, as shown in Figure S20b (Supporting Information). The Zn-MnO_2 full cell with Zn-NSCDs0.1 sustains a much longer cycle lifespan of 500 cycles and much higher Coulombic efficiency of nearly 99.5% than that using Zn-NSCDs0 which fails after ≈200 cycles. It is worth noting that the rate and cycling capacity increase might be attributed to the electrochemical activation process in the initial several cycles, which is a common phenomenon for the manganese-based electrodes.[46–48] Figure S21 (Supporting Information) shows the SEM images of the deposited Zn electrodes in Zn-NSCDs0 and Zn-NSCDs0.1 after 100 cycles, respectively. The former has massive sheet-like zinc dendrites, while the latter shows a dense and even surface without obvious dendrites formation. Furthermore, the Zn-MnO_2 battery self-discharge can be reflected by the CE of fully charged batteries after 24 h rest. An excellent CE of 96.3% is achieved in the cell with Zn-NSCDs0.1 (Figure 7e), while only 81.8% of the capacity is retained for the cell without NSCDs (Figure 7f). These results confirm that NSCDs do inhibit parasitic reactions and suppress Zn dendrites growth effectively during cycles.

3. Conclusion

Ultra-stable cycling performance of ZIBs is achieved by just adding a small amount of NSCDs into the common $ZnSO_4$ aqueous electrolyte. Such a kind of nitrogen-doped and sulfonated CDs exhibit multi-functions in ameliorating ZIBs. First, the abundant strong polar groups (-COOH, -NH_2, -OH, especially -SO_3H) on NSCDs are able to regulate the Zn^{2+} solvation structure by decreasing the coordinated active H_2O molecules. Second, partial NSCDs are adsorbed on Zn anodes to form a protective layer, which isolate the corrosion from H_2O/SO_4^{2-} and avoid side-reactions. Finally, the nitrogen species and the coordination groups of NSCDs attract Zn^{2+} and help them transfer rapidly on the surface, which induces a uniform electrolyte flux and a homogeneous Zn deposition.

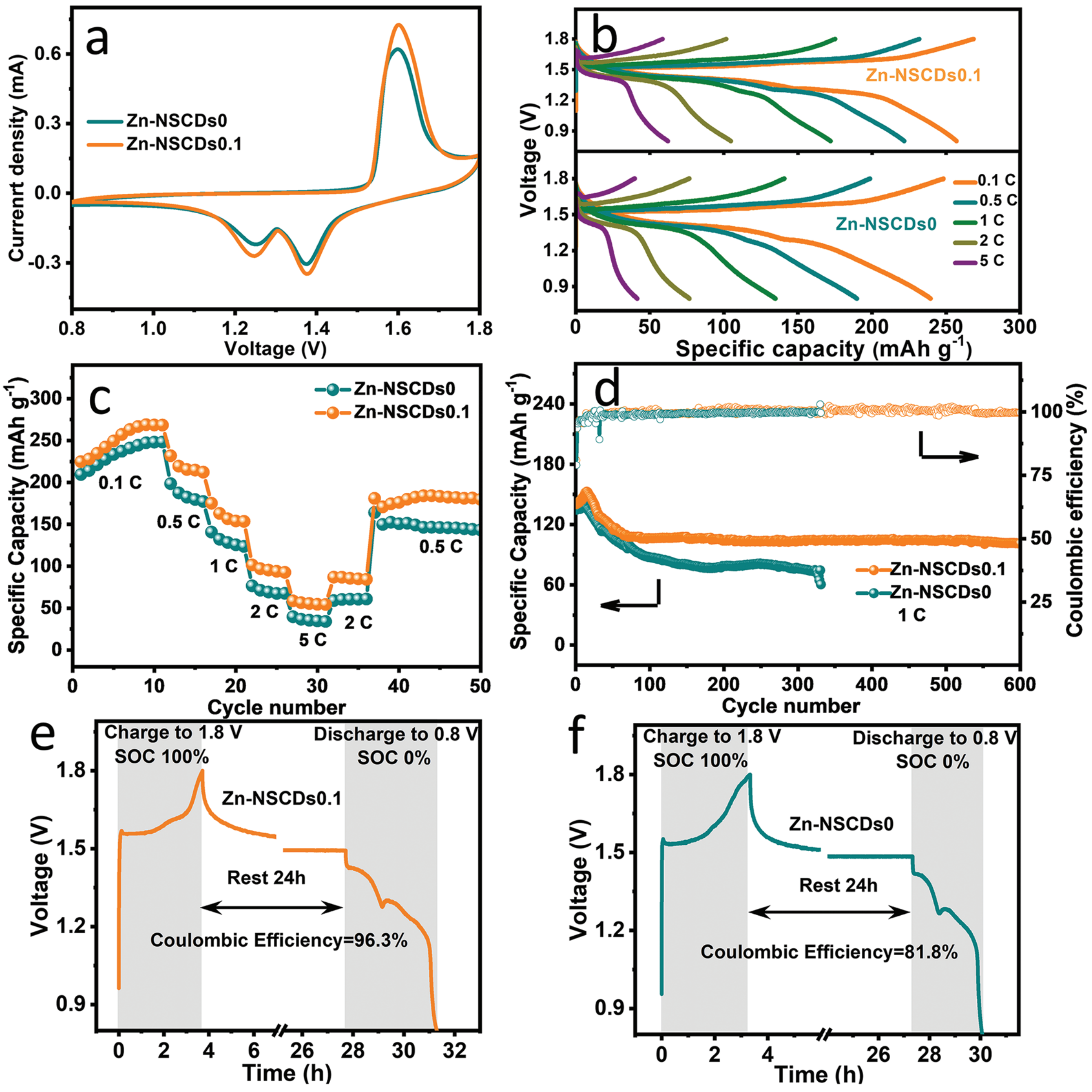

Figure 7. Electrochemical performance of Zn//MnO_2 cells in Zn-NSCDs0 and Zn-NSCDs0.1, respectively. a) CV curves at a scan rate of 0.1 mV s^{-1}. b) Charge-discharge curves and c) capacities variation under different current densities, respectively. d) Cyclic stability and Coulombic efficiency comparison at 1 C. Self-discharge analyses of Zn//MnO_2 cells using e) Zn-NSCDs0.1 and f) Zn-NSCDs0, respectively.

The above merits of NSCDs are supported by various characterizations and DFT calculations. As a result, both the Zn//Zn symmetric cells and the Zn//MnO_2 full cells with the $ZnSO_4$ aqueous electrolyte containing 0.1 mg mL^{-1} of NSCDs exhibit high reversibility and good rate performance during long-term cycles at room temperature. This work provides a very simple and effective method to improve ZIBs for the future practical applications.

4. Experimental Section

Preparation of NSCDs: NSCDs were prepared via a convenient solvothermal method. 1.728 g of citric acid and 0.7 g of metanilic acid were mixed in 20 mL of *N*, *N*-Dimethylformamide. The obtained solution was stirred for 30 min and poured into a Teflon-lined stainless-steel autoclave together with 600 µL of ethylenediamine at 160 °C for 5 h in an oven. Subsequently, the reactant solution was dispersed dropwise into ethanol to gather the brownness precipitate by high-speed centrifugation, followed by re-dissolving the precipitate in deionized water for dialysis of three days. The cutoff molecular weight of the dialysis bag was 3500. The dialyzed solution was freeze-dried to obtain NSCDs powder.

Preparation of MnO_2: The β-MnO_2 materials were fabricated by a facile hydrothermal method. 0.317 g of $KMnO_4$ and 2.03 g of $MnSO_4 \cdot H_2O$ were mixed in 40 mL of deionized water after continuous magnetic stirring for 30 min. The mixture was added into a Teflon-lined autoclave and maintained at 130 °C for 48 h. Then the precursor was washed and centrifuged by ethanol and deionized water. The obtained product was further dried at 100 °C for 48 h in a vacuum oven.

Characterization: The morphologies and structures of all materials were characterized by a transmission electron microscope (TEM, Tecnai G2 F20 S-Twin) and a scanning electron microscope (SEM, Zeiss Supra 55 and Phenom Prox). The X-ray diffraction (XRD) patterns were done on X-ray diffractometer (Bruker D2 Endeavor). Fourier transform infrared (FT-IR) spectra of powder samples and electrolytes were collected on Thermo Fisher Nicolet iS10 spectrometer and Thermo Fisher Nicolet6700 spectrometer, respectively. The fluorescence spectra were measured on a Horiba Jobin Yvon FluoroMax-4 spectrofluorometer. X-ray photoelectron spectroscopy (XPS) was recorded on a PHI 5000C&PHI5300 spectrometer.

Electrochemical Measurements: Zn//Zn symmetric cells were assembled using two pieces of Zn plates with a thickness of 100 µm as the working and the counter electrodes. The constant current densities were applied ranging from 0.5, 1, 2, 5 mA cm^{-2} and the charging/discharging times were employed to be 0.5 h. Zn//Ti half cells were fabricated to measure the Coulombic efficiency of Zn metal in different electrolytes with a Ti foil as the working electrode and a Zn plate as the counter electrode.

Zn//MnO$_2$ full cells were assembled using 2016-type coin cells at room temperature. The cathode was prepared by mixing 70 wt.% of β-MnO$_2$, 20 wt.% of acetylene black, and 10 wt.% of PVDF in *N*-methyl-2-pyrrolidone. The mixture was magnetically stirred for 4 h to form a uniform slurry, cast on a stainless-steel slice, then dried at 60 °C for 12 h in vacuum. The average active material of the electrode plate (12 mm in diameter) was ≈1.5–2 mg cm^{-2}. 80 µL of the electrolyte (Zn-NSCDsx) was added into each coin cell (Zn//Zn symmetric cells, Zn//Ti half cells, or Zn//MnO$_2$ full cells) with a piece of glass fiber (Whatman/D) as the separator, respectively. A three-electrode electrolysis bath was used to test the electrochemical potential window with a scan rate of 1 mV s^{-1}, in which two steel-meshes were employed as the working electrode and the counter electrode respectively, and Ag/AgCl electrode was employed as the reference electrode. When measuring Tafel plots in the range of –0.7—1.2 V at a scan rate of 1 mV s^{-1}, two Zn plates were used as the working electrode and the counter electrode respectively, with a reference electrode of Ag/AgCl. The cyclic voltammetry (CV), the electrochemical impedance spectroscopy (EIS), the electrochemical potential windows, and the Tafel plots were respectively carried out by an electrochemical workstation (Chenhua CHI 660E). The chronoamperometry (CA) was measured on a multichannel electrochemical workstation (Bio-Logic VSP-300). The galvanostatic charge/discharge (GCD) tests at different current densities were performed on a LAND CT2001A cell testing system.

Density Functional Theory (DFT) Calculations: All structural optimization and total energy calculations were carried out with Gaussian 09 at the level of PBE/6-31G*.[49,50] For each optimized geometry of the functionalized NSCDs bonded with Zn^{2+}, the binding energy defined as $E_b = E_{total} - E_{sub} - EZn^{2+}$, was calculated with the basic set superposition error corrected by the counterpoise method. E_{sub}, EZn^{2+} and E_{total} represent the energies of one empty substrate, a single Zn^{2+} ion, and the total energy of the complex, respectively.

Supporting Information

Supporting Information is available from the Wiley Online Library or from the author.

Acknowledgements

This work was financially supported by the National Natural Science Foundation of China (21975048, 21771039), and the Shanghai Science and Technology Committee (19DZ2270100).

Conflict of Interest

The authors declare no conflict of interest.

Data Availability Statement

The data that support the findings of this study are available in the supplementary material of this article.

Keywords

additive, carbon dots, electrolytes, multifunctional, zinc-ion batteries

Received: September 8, 2022
Revised: November 15, 2022
Published online: January 17, 2023

---

[1] J. Cao, D. Zhang, X. Zhang, Z. Zeng, J. Qin, Y. Huang, *Energy Environ. Sci.* **2022**, *15*, 499.
[2] J. Hao, X. Li, S. Zhang, F. Yang, X. Zeng, S. Zhang, G. Bo, C. Wang, Z. Guo, *Adv. Funct. Mater.* **2020**, *30*, 2001263.
[3] T. C. Li, D. Fang, J. Zhang, X. L. Li, E. P. Mei, Y. L. Zhi, J. Yu, Y. Dong, H. Y. Yang, *J. Mater. Chem.* **2021**, *9*, 6013.
[4] P. Ruan, S. Liang, B. Lu, H. J. Fan, J. Zhou, *Angew. Chem., Int. Ed.* **2022**, *61*, 202200598.
[5] N. Dubouis, A. Serva, E. Salager, M. Deschamps, A. Grimaud, *J. Phys. Chem. Lett.* **2018**,*9*, 6683.
[6] J. Wang, Y. Yang, Y. Zhang, Y. Li, H. Wang, *Energy Storage Mater.* **2021**, *35*, 19.
[7] A. Liu, F. Wu, Y. Zhang, J. Zhou, Y. Zhou, M. Xie, *Small* **2022**, *18*, 2201011.
[8] D. Chao, W. Zhou, F. Xie, C. Ye, S. Z. Qiao, *Sci. Adv.* **2020**, *6*, aba4098.
[9] X. Yang, C. Li, Z. Sun, S. Yang, J. Sun, *Adv. Mater.* **2021**, *33*, 2105951.
[10] Y. Liu, Q. Shi, Y. Wu, Q. Wang, P. Chen, *Chem. Eng. J.* **2020**, *407*, 127189.
[11] Y. Jin, K. S. Han, Y. Shao, M. L. Sushko, J. Xiao, H. Pan, J. Liu, *Adv. Funct. Mater.* **2020**, *30*, 2003932.
[12] R. Yao, L. Qian, Y. Sui, G. Zhao, R. Guo, S. Hu, P. Liu, H. Zhu, F. Wang, C. Zhi, *Adv. Energy Mater.* **2022**, *12*, 2102780.
[13] S. Guo, L. Qin, T. Zhang, M. Zhou, S. Liang, *Energy Storage Mater.* **2021**, *34*, 545.
[14] T. B. Song, Z. H. Huang, X. Q. Niu, X. R. Zhang, J. S. Wei, H. M. Xiong, *ChemSusChem* **2022**, *15*, 202102390.
[15] S. Li, Z. Luo, H. Tu, H. Zhang, W. Deng, G. Zou, H. Hou, X. Ji, *Energy Storage Mater.* **2021**, *42*, 679.
[16] T. B. Song, Z. H. Huang, X. Q. Niu, J. Liu, J. S. Wei, X. B. Chen, H. M. Xiong, *ChemNanoMat* **2020**, *6*, 1421.
[17] J. S. Wei, T. B. Song, P. Zhang, X. Q. Niu, X. B. Chen, H. M. Xiong, *Mater. Chem. Front.* **2020**, *4*, 729.
[18] J. S. Wei, H. Ding, P. Zhang, Y. F. Song, J. Chen, Y. G. Wang, H. M. Xiong, *Small* **2016**, *12*, 5927.
[19] J. S. Wei, Z. Y. Zhu, X. Zhao, T. B. Song, J. H. Huang, Y. X. Zhang, X. Liu, L. Chen, X. Q. Niu, Y. G. Wang, H. M. Xiong, *Chem. Eng. J.* **2021**, *425*, 130660.
[20] Z. Y. Zhu, J. S. Wei, J. Huang, X. Dong, P. Zhang, H. M. Xiong, *J. Inorg. Mater.* **2020**, *35*, 423.
[21] H. Zhang, R. Guo, S. Li, C. Liu, H. Li, G. Zou, J. Hu, H. Hou, X. Ji, *Nano Energy* **2022**, *92*, 106752.
[22] H. Zhang, S. Li, L. Xu, R. Momen, W. Deng, J. Hu, G. Zou, H. Hou, X. Ji, *Adv. Energy Mater.* **2022**, *12*, 2200665.
[23] W. Han, H. Lee, Y. Liu, Y. Kim, H. Chu, G. Liu, W. Yang, *Chem. Eng. J.* **2023**, *452*, 139090.
[24] R. V. Nair, P. R. Chandran, A. P. Mohamed, S. Pillai, *Anal. Chim. Acta* **2021**, *1181*, 338893.
[25] M. Moniruzzaman, J. Kim, *Appl. Surf. Sci.* **2021**, *552*, 149372.
[26] Y. Zhu, J. Li, X. Yun, G. Zhao, X. Ji, *Nano-Micro Lett.* **2020**, *12*, 16.
[27] S. Qin, X. Yu, L. Xu, *J. Hazard. Mater.* **2020**, *405*, 123978.
[28] M. Pajewska-Szmyt, B. Buszewski, R. Gadzaa-Kopciuch, *Mater. Chem. Phys.* **2019**, *242*, 122484.
[29] D. Hong, Y. Choi, J. Ryu, J. Mun, W. Choi, M. Park, Y. Lee, N. S. Choi, G. Lee, B.-S. Kim, S. Park, *J. Mater. Chem. A* **2019**, *7*, 20325.

[30] J. Wolska, K. Stawicka, J. Walkowiak-Kulikowska, *Mater. Chem. Phys.* **2021**, *273*, 125132.

[31] K. S. Siow, L. Britcher, S. Kumar, H. Griesser, *Sains Malays.* **2018**, *47*, 1913.

[32] Z. Cao, X. Zhu, S. Gao, D. Xu, Z. Wang, Z. Ye, L. Wang, B. Chen, L. Li, M. Ye, *Small* **2021**, *18*, 2103345.

[33] J. Pavelec, D. Diguiseppi, B. Y. Zavlavsky, V. N. Uversky, R. Schweitzer-Stenner, *J. Mol. Liq.* **2019**, *275*, 463.

[34] P. Sun, L. Ma, W. Zhou, M. Qiu, Z. Wang, D. Chao, W. Mai, *Angew. Chem., Int. Ed.* **2021**, *133*, 2.

[35] J. Hao, L. Yuan, C. Ye, D. Chao, K. Davey, Z. Guo, S. Qiao, *Angew. Chem., Int. Ed.* **2021**, *60*, 7366.

[36] N. Chang, T. Li, R. Li, S. Wang, Y. Yin, H. Zhang, X. Li, *Energy Environ. Sci.* **2020**, *13*, 3527.

[37] B. Wang, R. Zheng, W. Yang, X. Han, C. Hou, Q. Zhang, Y. Li, K. Li, H. Wang, *Adv. Funct. Mater.* **2022**, *32*, 2112693.

[38] L. Zhang, L. Miao, W. Xin, H. Peng, A. Z. Yan, Z. Zhu, *Energy Storage Mater.* **2022**, *44*, 408.

[39] Y. Chu, S. Zhang, S. Wu, Z. Hu, G. Cui, J. Luo, *Energy Environ. Sci.* **2021**, *14*, 3609.

[40] Y. Wang, Y. Wang, C. Chen, X. Chen, Q. Zhao, L. Yang, L. Yao, R. Qin, H. Wu, Z. Jiang, F. Pan, *Chem. Commun.* **2021**, *57*, 5326.

[41] N. H. Andersen, P. Bandaranayake, M. A. Careem, M. Dissanayake, C. N. Wijayasekera, R. Kaber, A. Lundén, B. E. Mellander, L. Nilsson, J. O. Thomas, *Solid State Ionics* **1992**, *57*, 203.

[42] S. J. Zhang, J. Hao, D. Luo, P. F. Zhang, B. Zhang, K. Davey, Z. Lin, S. Z. Qiao, *Adv. Energy Mater.* **2021**, *11*, 2102010.

[43] M. Han, J. Huang, X. Xie, T. C. Li, J. Huang, S. Liang, J. Zhou, H. J. Fan, *Adv. Funct. Mater.* **2022**, *32*, 2110957.

[44] A. Bayaguud, X. Luo, Y. Fu, C. Zhu, *ACS Energy Lett.* **2020**, *5*, 3012.

[45] L. Cao, D. Li, E. Hu, J. Xu, T. Deng, L. Ma, Y. Wang, X. Q. Yang, C. Wang, *J. Am. Chem. Soc.* **2020**, *142*, 21404.

[46] D. Zhao, Z. Zhang, J. Ren, Y. Xu, X. Xu, J. Zhou, F. Gao, H. Tang, S. Liu, Z. Wang, D. Wang, Y. Wu, X. Liu, Y. Zhang, *Chem. Eng. J.* **2023**, *451*, 138882.

[47] F. Gao, B. Mei, X. Xu, J. Ren, D. Zhao, Z. Zhang, Z. Wang, Y. Wu, X. Liu, Y. Zhang, *Chem. Eng. J.* **2022**, *448*, 137742.

[48] C. Wang, Z. Wang, D. Zhao, J. Ren, S. Liu, H. Tang, P. Xu, F. Gao, X. Yue, H. Yang, C. Niu, W. Chu, D. Wang, X. Liu, Z. Wang, Y. Wu, Y. Zhang, *ACS Appl. Mater. Interfaces* **2021**, *13*, 55020.

[49] M. J. Frish, G. W. Trucks, H. B. Schlegel, G. E. Scuseria, M. A. Robb, J. R. Cheeseman, G. Scalmani, V. Barone, G. A. Petersson, H. Nakatsuji, et al., Gaussian 09, Revision D.01, Gaussian, Inc., Wallingford, CT **2009**.

[50] J. P. Perdew, K. Burke, M. Ernzerhof, *Phys. Rev. Lett.* **1996**, *78*, 3865.